J Mater Sci: Mater Electron (2016) 27:6992–7003
DOI 10.1007/s10854-016-4655-6

Significant development on pinning of vortices in Y-123 superconductor with homovalent Ba/Nd substitution

Namik Kemal Saritekin[1] · Muhammed Oz[2] · Cabir Terzioglu[1] · Osman Gorur[1] · Gurcan Yildirim[3]

Received: 29 January 2016 / Accepted: 7 March 2016 / Published online: 15 March 2016

Abstract In this study, the magnetotransport measurements are performed in the field range of 0–7 T to determine the effect of Nd nanoparticles inserted in the Y-123 crystal structure on the superconducting characteristics and flux pinning mechanism of the $YBa_{2-y}Nd_yCu_3O_7$ materials ($0.000 \leq y \leq 0.500$). Moreover, the experimental measurement results enable us to evaluate the crucial parameters as regards critical transition temperatures (T_c^{onset} and T_c^{offset}), room temperature resistivities (ρ_{300}), residual resistivity ratios (RRR), thermodynamic critical fields ($\mu_0 H_c$), lower critical fields ($\mu_0 H_{c1}$), upper critical fields ($\mu_0 H_{c2}$), critical fields ($\mu_0 H_{c3}$), irreversibility fields ($\mu_0 H_{irr}$), coherence lengths (ξ), penetration depths (λ) and Ginzburg–Landau (κ) parameters. All the values obtained show the considerable improvement with the increment of the Nd nanoparticles in the Y-123 crystal system up to the critical value of $y = 0.250$ beyond which the prompt degradation begins in the crystal structure due to new induced artificial dislocations and permanent disorders in the Cu–O_2 consecutively stacked layers. Hence, the excess Nd inclusions lead to the thermal motion of the vortices easily. This fact is completely confirmed by the magnetotransport measurements performed in the external magnetic fields. Namely, the optimum level of Nd dopant seriously increases the coupled regions as a result of the degradation of pancake positional fluctuations, and pinning of two-dimensional pancake vortices enhances with the recoupling of the adjacent layers. However in case of the maximum Nd inclusions, the flattened pancakes with more interplane interaction energy never travel from layer to layer due to the alteration of the coupled vortices into the discrete pancakelike (recoupling linelike) nature. In other words, the excess Nd nanoparticles inserted in the Y-123 crystal system reduce significantly the interlayer Josephson coupling length, elastic moduli of the vortex lattice and magnetic field carrying capacity. Furthermore, the flux pinning energy (U_0) is calculated from thermally activated flux flow model. The activation energy computed increases regularly with the increment of Nd decorations until $y = 0.250$ after which the value significantly decreases towards to the global minimum point. However, the pinning energy values always decrease with the increase of the external magnetic field strength. In case of external magnetic fields of 7 T the maximum activation energy is found to be about 477 K. As for the Y-123 material doped with maximum Nd additives of $y = 0.500$, the flux pinning energy values are not calculated at any applied magnetic field which is >0.1 T due to the cooper pair-breaking in Ba-site Nd substituted Y-123 systems. At the same time, the evaluated parameters follow the same trend: firstly enhancement up to the critical Nd dopant value of $y = 0.250$ and then the rapid regression towards the global minimum point. Finally, the optimum Nd impurity level is found to be $y = 0.250$ in the Y-123 system at even higher applied magnetic field strengths.

✉ Namik Kemal Saritekin
tekinfizikster@gmail.com

[1] Department of Physics, Abant Izzet Baysal University, 14280 Bolu, Turkey

[2] Gerede Vocational School, Abant Izzet Baysal University, 14280 Bolu, Turkey

[3] Department of Mechanical Engineering, Abant Izzet Baysal University, 14280 Bolu, Turkey

1 Introduction

Application of Y-based high temperature superconducting compounds in high magnetic fields and temperatures is restricted due to strong anisotropic property, very low

charge carrier density, large penetration depth and short coherence length [1, 2]. However, the materials are especially preferred in researches and applications used in industry and technology because of their intrinsic optical and electronic properties, high transition temperature, smaller power losses, their remarkable high current and magnetic field carrying capacity [3, 4]. It is well known that the slight variations in the crystalline configuration of a high temperature cuprate superconductor (HTCS) form major changes in its magnetic properties [5]. In this respect, the chemical doping and substitutions of cations or anions are generally used for the structural variations [6] as a result of the alteration of the location and occupancy of the atoms positioned in the charge reservoirs CuO or Cu–O_2 consecutively stacked layers. Similarly the superconducting transition temperature (abbreviated as T_c) increases or decreases considerably [7–11]. Moreover, the structure of a HTCS can be changed by altering the vacancy of the oxygen atoms in the charge reservoirs. When the oxygen content of superconductor $YBa_2Cu_3O_7$ (Y-123) is lesser than the amount of 6.4, the crystalline structure changes from orthorhombic Pmmm lattice structure to tetragonal P4/mmm lattice structure as antiferromagnetic insulator. On the other hand, the maximum J_c peak occurs in J_c versus applied magnetic field graph owing to structural defects such as intrinsic pinning of vortices at the Cu–O_2 planes [12] or oxygen vacancy clusters [13, 14]. This is known as the peak effect [15, 16]. It is thought that parameter of J_c decreases with increasing temperature as a consequence of the enhanced heat activity (flux movement) in the superconducting system. Accordingly, the flux pinning is strong in low temperature. Furthermore, the J_c values rely sensitively on the impurity in superconducting matrix, and high J_c parameter is observed in the presence of large local flux pinning centers. The long and short of it is that both the Jc and T_c values of the superconductor depend strongly on the substitution and doping concentration.

The activation energy directly related to the pinning ability is defined as a measure of flux pinning strength of a superconductor material [17, 18]. The flux pinning energy value is calculated from the thermally assisted flux flow (TAFF) model described by Arrhenius equation.

In the current work, we exert the magnetoresistivity measurements of a bulk $YBa_{2-y}Nd_yCu_3O_7$ samples among the applied magnetic field strengths of 0–7 T in the temperature range of 10–120 K to find any possible structural influences stemmed from the foreign nanoparticles. The crystal structures of bulk $YBa_{2-y}Nd_yCu_3O_7$ materials might be affected by grain boundaries, secondary phases and structural defects. Thus, we deduce the values of critical transition temperatures, critical fields, coherence lengths and penetration depths from the magnetoresistivity curves. Moreover, the flux pinning energy values of the $YBa_{2-y}Nd_yCu_3O_{7-\delta}$ samples studied are obtained with the aid of the TAFF model. As a result, both the critical temperature and activation energy values increase with the enhancement of Nd content up to $y = 0.250$ beyond which they decrease owing to the presence of excess magnetic ions. In other words, pair-breaking mechanism in the system plays dominant role on the degradation of the Y-123 phase formation [19].

2 Experimental details

In the previous study [20], the change of the structural, mechanical, electrical and superconducting properties with the Nd inclusions inserted in the Y-123 superconducting matrix is investigated according to bulk density, X-ray diffraction, scanning electron microscopy, dc resistivity, microhardness and transport critical current density measurements. The samples are prepared by solid-state reaction method. In the present study, we attempt to scrutinize the impact of the Nd impurities on the magnetoresistivity behavior of the Y-123 superconducting system by use of the zero field cooling (ZFC) procedure. Thus, the resistivity of all the samples decreases linearly in ZFC, and transition from superconducting to normal sample (T_c^{onset}) in ZFC is much clearer than T_c^{onset} in FC. The measurements with the four-probe method are made between 10 and 120 K by applying magnetic field in range 0–7 T and constant current of 5 mA. The external magnetic fields, which are perpendicular to the c-axis, are applied normal to the direction of the current. The critical transition temperatures (T_c^{onset} and T_c^{offset}), room temperature resistivity (ρ_{300K}), residual resistivity ratio (*RRR*), irreversibility field (μ_0H_{irr}), upper critical field (μ_0H_{c2}), thermodynamic critical field (μ_0H_c), activation energy (U_0), penetration depth (λ), coherence length (ξ) and Ginzburg–Landau (κ) parameters are calculated from the experimental magnetoresistivity graphs. In this paper, we represent the undoped sample as Nd0 and Nd stoichiometries such as 0.025, 0.050, 0.100, 0.250 and 0.500 in the Ba-site Nd substituted Y-123 superconductor are called Nd1, Nd2, Nd3, Nd4 and Nd5, respectively.

3 Results and discussion

3.1 Magnetoresistivity measurement results

The magnetotransport measurement findings constitute the main part of this paper due to the crucial parameters (T_c^{onset}, T_c^{offset}, ρ_{300K}, *RRR*, μ_0H_{irr}, μ_0H_{c2}, μ_0H_c, U_0, λ, ξ and κ) evaluated from the experimental results. In this work, the

effects of Nd foreign nanoparticles on the magnetoresistivity characteristics are investigated at various external fields (0 T $\leq$ H $\leq$ 7 T). Figure 1 shows the experimental magnetoresistivity curves for the pristine and Ba-site Nd substituted Y-123 superconductor. It is visible from the figure that both the offset and onset transition critical temperature values tend to increase with the increment in the Nd concentration level up to the certain value of y = 0.250 above which the value (especially T_c^{offset}) reduces towards to the global minimum value for the maximum content level of Nd impurity due to new induced artificial dislocations (lattice defects), bulk defects (cracks, voids and pores) and permanent disorders in orientation of consecutively stacked layers [21, 22]. On the other hand, the T_c^{offset} values decrease considerably as a consequence of the fluxion motions along with adjacent layers by the enhancement of the external magnetic field applied whereas the T_c^{onset} values are hardly affected due to the intrinsic superconducting characteristics of the Y-123 compound [23]. Based on the combination of the Nd concentration level and applied magnetic fields, it is fair to conclude that the excess Nd additions in the Y-123 superconducting system lead to not only reduction in the coupling property of the cooper-pairs, and structural inhomogeneities in the oxidation state of the inter-grains and grain boundaries but also enhancement of the weak connectivity between the superconducting grains under the external magnetic fields (Fig. 1) [24]. In numerically, the maximum T_c^{offset} (T_c^{onset}) value is observed to be about 97.25 K (98.93 K) for the Nd4 superconducting sample while the minimum value is 32.97 K (54.84 K) for the Nd5 compound at zero applied magnetic fields. What stands out clearly here that the excess Nd decorations in the Y-123 superconducting matrix lessen considerably the mobile hole concentrations [25, 26].

As for the magnetotransport measurements, the external field strengths suppress the critical transition temperature values for the $YBa_{2-y}Nd_yCu_3O_{7-\delta}$. Abrikosov and Gorkov (AG) explained the suppression in the critical transition temperatures with the pair-breaking theory in which the interaction between the magnetic impurities of spin S and conduction electron spins in the Cooper pairs makes the change in the spin states of the electrons and hence the Cooper pairs tend to break suddenly [27]. Furthermore, the significant decrement in T_c^{offset} parameter is associated with the increment of de Gennes factor ($G = (g-1)^2 J(J+1)$) consisting of Lande g factor and total angular momentum for the Hund's rules in the ground state owing to the presence of the magnetic impurities in the system. In this work, the excess magnetic Nd impurities (magnetic moments) result in the hole filling (localization) in the conduction band [28–30] as a result of the hybridization (cooper-pair breaking mechanism) of Cu3d–O_2p states in the Cu–O_2 layers [31–34]. As for the experimental findings under the external magnetic field strengths, the T_c^{offset} value of pristine material decreases from 84.52 to 53.10 K with the increasement of the applied magnetic field up to the constant field of 7 T. Similarly, the value of best (Nd4) sample is felt down to 82.04 K. In fact, we could not measure the offset critical transition temperature value of the Nd5 compound after the external field strength of 0.1 T due to the destruction of the superconducting properties. It is to be mentioned here that each T_c^{offset} parameter is much more lowered as compared to the T_c^{onset} parameter with the increment of Nd foreign impurities and especially applied magnetic field. Under these circumstances, do the T_c^{onset} values pertaining to the superconducting materials hardly alter when the T_c^{offset} values decrease dramatically. Namely, the degree of broadening (variation of ΔT_c) for the virgin and best materials is observed to be about 41.59 and 16.89 K, respectively with the increment in the applied magnetic field. Shortly, the enhancement of the applied magnetic field perpendicular to the c-axis brings about an extensive broadening of the superconducting transition due to the decrement in the flux pinning ability of the superconducting samples [35] as a result of the dissipation defined by the TAFF [8]. Moreover, the crucial results of measurements performed at the applied magnetic fields confirm that the retrogression in the pinning of two-dimensional 2D pancake vortices (improvement in the recoupling linelike) stems from both the presence of the decoupling of the adjacent layers and the suppression of the interlayer Josephson coupling with the Nd substitution level in the crystal textures [36]. The decrement of T_c^{offset} with increment of magnetic field applied stems from the grain boundary weak-links arisen from porosity and non-superconducting phases. Magnetic field begins to enter into the grain boundary weak-links and harms the superconducting properties seriously. Besides, the Nd^{+3} with strong magnetic ions exhibits high value of magnetic moment in the same direction of the magnetic field applied. Thus, the magnetic impurities inserted in the crystal structure increase the interior magnetic field. This is known as the main reason of decrease in the T_c^{onset} and T_c^{offset} values.

It is another probable result obtained from Fig. 1 that the $YBa_{2-y}Nd_yCu_3O_{7-\delta}$ samples studied exhibit the positive temperature derivative of the resistivity (metallic behavior resulting from the interactions between the electron and phonon in the crystal lattice or the logarithmic divergence in density of states at the Fermi level) above their own critical temperature values [37, 38]. The room temperature resistivity (ρ_{300K}) value tends to decrease with increasing the Nd inclusions in the Y-123 crystal structure up to the concentration level of y = 0.250 after which the ρ_{300K}

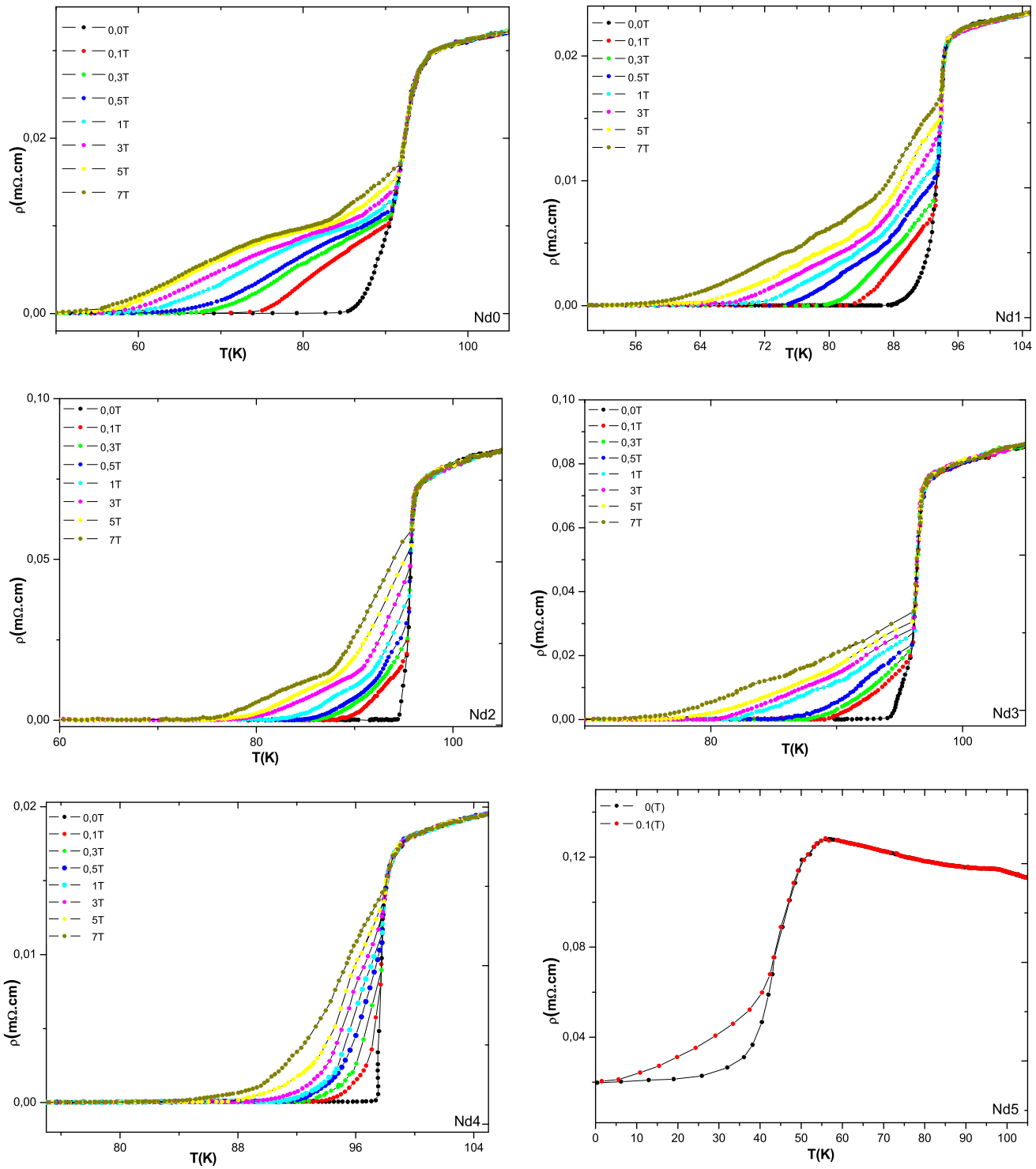

Fig. 1 Change of magnetoresistivity against temperature at several applied magnetic fields in the range of 0–7 T

value immediately increases by three times and reaches to the maximum value of 8.61 mΩ cm. The regular decrease of normal state resistivity is attributed to the increment of both the metallic interactions between the superconducting grains and optimization of the mobile hole carrier concentration in the Cu-O_2 slabs [39].

The magnetoresistivity curves allow us to determine the temperature-independent residual resistivity (ρ_0) and residual resistivity ratio (RRR) seriously. As well known, the former parameter deduced from the extrapolation method ascribes to the defects stemming from the grain boundary weak-links or possibly additional scattering

centers [40, 41]; on the other hand, the latter one obtained from the ratio of ρ_{300K}/ρ_{95K} is in accordance with the determinant of the sample quality [42].

The ρ_{300K} and RRR values deduced for the materials studied in this comprehensive work are numerically tabulated in Table 1. It is apparent from the figure that the ρ_{300K} values are found to decrease from 7.89 to 2.77 mΩ cm with the enhancement of the Nd decorations in the superconducting system up to the content value of y = 0.250. This is associated with the decrement of impurity scattering and random defects regarding the superconducting grain boundaries, stacking faults, planar voids, cracks and micro defects in the Cu–O_2 planes [43]. As for the latter (RRR) parameters, the Nd4 material obtains value of 173 while the smallest value of 0.75 is observed for the Nd5 sample. It is pertinent to mention here that the Nd4 compound with the greatest conductivity is produced in the best quality.

The grain sizes are in the nm scale and they are more uniform than pure YBCO up to y = 0.250. The mean crystallite diameter obtained from XRD analysis (not shown here) using the Scherer's formula [44] is 93 nm. The fact that nearly uniform grain sizes have been obtained after the preparation of the sample is important for the magnetic analysis. Non-regular grains imply grain boundaries with different areas and thus less uniform Josephson junctions between superconducting grains.

We now focus on studying the magnetic features of the $YBa_{2-y}Nd_yCu_3O_7$ and any relationship with the structural characteristics of samples. Meanwhile, $YBa_{2-y}Nd_yCu_3O_7$ is a type II superconductor, some of its elementary properties can be pronounced by the field-dependence magnetization, $M(H)$, which also provides information about the trapped fields in it. This behavior is caused by the paramagnetic characteristic of its secondary phases such as Y_2BaCuO_5, CuO and $BaCuO_2$. The presence of impurities or secondary phases in samples is detected by analyzing their magnetization curves as the temperature approaches T_c. The $M(H)$ dependence for the clean and defect-free cuprate superconductors is noted to be reversible. Namely, no magnetic flux is trapped within the superconductor as disappearance of the external field. The $M(H)$ dependence becomes highly irreversible for superconductors containing defects or impurities which interact with the penetrating flux lines. Secondary phases are commonly found after the preparation of HTCSs. The phases obtained for YBCO by the preparation technique (solid state) are Y_2BaCuO_5, CuO and $BaCuO_2$ [45]. The presence of secondary phases is a possible explanation for the origin of the fishtail or peak effect [46, 47]. In the case of $YBa_{2-y}Nd_yCu_3O_7$, such decrease affects the critical current density values, the pinning force and could be caused by structural defects like partial occupancy of the oxygen in the Cu–O chains in the structure. The irreversible magnetization is zero at $H = H_{irr}$, in contrast to the reversible magnetization disappearing at $H = H_{c2}$. Ultimately, as the external field is reduced from H_{c2} to H_{c1} the magnetic moment becomes positive over a wide range of applied field indicating that not much magnetic field has been trapped in the $YBa_{2-y}Nd_yCu_3O_7$ superconductor as in YBCO. Therefore two characteristics can be observed from the ρ-T graph, the irreversibility and remnant magnetization are caused by presence of secondary phases whereas the decrease of magnetization under external field is possibly caused by structural defects.

The critical current density of a bulk superconducting compound with randomly oriented grains is strongly limited due to the weak link behavior. Only very small currents are able to flow throughout the grain boundaries when the external magnetic field is applied. This dependence is dominated by the classical $1/H$ law [48] reflecting the $J_c(H)$ dependence of a percolation network of Josephson junctions [49].

The peak effect in YBCO is correlated with clustering of the oxygen vacancies. The J_c is controlled by two contributions, the background contribution of inter-grain currents of a bulk sample and the intra-grain contribution of field-induced pinning (originating the peak effect) which might be caused by clusters of oxygen vacancies in the Cu–O chains. The latest is better seen when the temperature is closer to T_c.

Table 1 Electrical measurement results including ρ_{300K}, *RRR*, T_c^{onset} and T_c^{offset} results of the $YBa_{2-y}Nd_yCu_3O_{7-\delta}$ samples under different external magnetic fields

Samples	T_c^{onset} (K)	T_c^{offset} (K)								Resistivity at 300 K mΩ cm	RRR (ρ_{300K}/ρ_{95K})
		0 T	0.1 T	0.3 T	0.5 T	1 T	3 T	5 T	7 T		
YNd0	94.69	84.52	74.95	68.19	64.29	61.03	58.57	56.40	53.10	7.89	2.68
YNd1	95.41	88.44	82.96	79.93	75.22	71.62	67.66	63.82	57.71	7.45	3.48
YNd2	96.90	93.62	88.27	85.96	84.83	81.90	77.50	75.92	73.22	6.5	3.69
YNd3	98.13	94.88	89.24	87.18	85.89	80.89	80.94	80.15	74.94	4.19	3.81
YNd4	98.93	97.25	92.96	92.69	91.10	90.71	89.01	87.44	82.04	2.77	173
YNd5	54.84	32.97	0	Not measurable						8.61	0.75

3.2 Activation energy

It is known with certainty that the copper oxide plane carries the maximum value of current while the current is the minimum value through the layers perpendicular to the Cu–O_2 plane. In high temperature superconductors, coherence length is very small from penetration depth. As the lower critical magnetic field B_{C1} of high-temperature superconductors is very low, the upper critical magnetic field B_{C2} value is very high. Thus, fixing the magnetic vortex weakened and in this case the critical current Ic decreases. The size of the energy barrier for fluksoid of new oxide superconductors is smaller than conventional superconductors and it is determined that a small coherence length cause the small energy barrier [50]. Unlike almost all low-temperature superconductors are isotropic, high temperature superconductor shows a high spatial anisotropy. Anisotropy shows itself in critical fields, critical current density, the depth of penetration of the magnetic field and resistance measurement. Anisotropy occurs mainly due to the layered crystal structure that is the default for superconductivity of high temperature. Free porosity, high density, strong links between particles and homogeneous structure able to be formed for superconducting material are important as building features.

The Y-based superconductors exhibit extremely weak flux pinning characteristic due to their inherent anisotropy. Even, the presence of vortices in the system prevents to pass larger currents along the materials at rather smaller magnetic field applied. The increment in the external field applied result in decrement slowly the vortex lattice period but increase the density of the vortices owing to the change in the nature of flux-line motion.

As a result, the pinning of two-dimensional (2D) pancake vortices recrudesces owing to the decoupling of the adjacent layers, and so the sample starts to show the resistivity. Namely, the excess Nd impurities deteriorate essentially the interlayer Josephson coupling by ascending the thermal fluctuations of pancake positions. The magnetic field carrying capacity is considerably retrograded by the decrease of Josephson coupling length and the increase in the elastic moduli of the vortex lattice [36]. Theoretically, the thermal activation creates the flux lines jump to neighboring states over the energy barriers (called as the statistical distribution) [51, 52] and so extra electrical energy recommended by Arrhenius law transforms into the heat energy [53].

Furthermore, thermally activated flux flow (TAFF) is strong method to scrutinize the pinning (dissipation) mechanism and potential energy barriers of the pinning centers in the Y-123 superconducting materials [54, 55]. In this work, the magnetic field dependence of the effective flux pinning (activation) energy values is determined from Arrhenius activation law abbreviated as $\rho = \rho_0 \exp\left(-U_0/k_B T\right)$. In the model, when U_0 symbolizes the pinning energy value, k_B is the universal Boltzmann's constant and ρ_0 is a field-independent pre-exponential factor [56]. The flux pinning energy values of our superconducting ceramics samples are obtained from the slope of linear data in the broadening tail part of Arrhenius graphs (variation of logarithmic resistivity over the reciprocal of temperature) at different applied magnetic fields in the range of 0–7 T as given in Fig. 2. The energy dissipation is steady with the thermal activation of flux across the pinning barrier. Interestingly, the figure demonstrates that the flux pinning energy values are dependent strongly upon the Nd concentration level and external magnetic field. In more detail, all the activation energy values deduced are numerically listed in Table 2. According to the table given, the activation energies tend to decrease considerably with the increase of applied magnetic fields. To illustrate, the energy values pertaining to the Nd4 sample is computed to be about 6997 and 477 K at zero and 7 T applied magnetic field, respectively. Similarly, the value is found to be about 86 K (53 K) at zero (0.1 T) magnetic field applied for the Nd5 sample. The substantial decrement in the pinning energy values are related to the contraction of distance between the pinning centers, confirming the presence of different superconducting levels within the superconducting materials at the inter-granular regions [57, 58]. In other words, the excess Nd impurities degrade significantly the energy barriers in the adjacent layers [59].

Additionally, the flux pinning energy values with regard to various applied magnetic fields are graphically given in Fig. 3. While the flux pinning energy values are decreasing sharply up to the certain magnetic field value of about 1 T, they reduce slowly and slowly above it. The main reason of this behavior stems from the penetration of the magnetic field into only the inter-granular media below the field value of 1 T [60].

Moreover, we survey the magnetic field dependence of the flux pining energies belonging to the $YBa_{2-y}Nd_yCu_{3-}O_{7-\delta}$ compounds with the aid of the log–log plot of activation energy versus applied magnetic field (Fig. 4). It is obvious from the figure that the relation between the variables is obtained to be linear and the external field-dependence of the flux pinning energy can thus be defined by a power law as:

$$U(\mu_0 H) \propto \mu_0 H^{-\beta} \quad (1)$$

here the parameter of β is in association with the orientation of the magnetic field in terms of the basal plane and magnetic field strength. After fitting the data obtained, we find the β values in the range from 0.486 (for the Nd0 sample) to 0.307 (for the Nd4 material) as embedded in

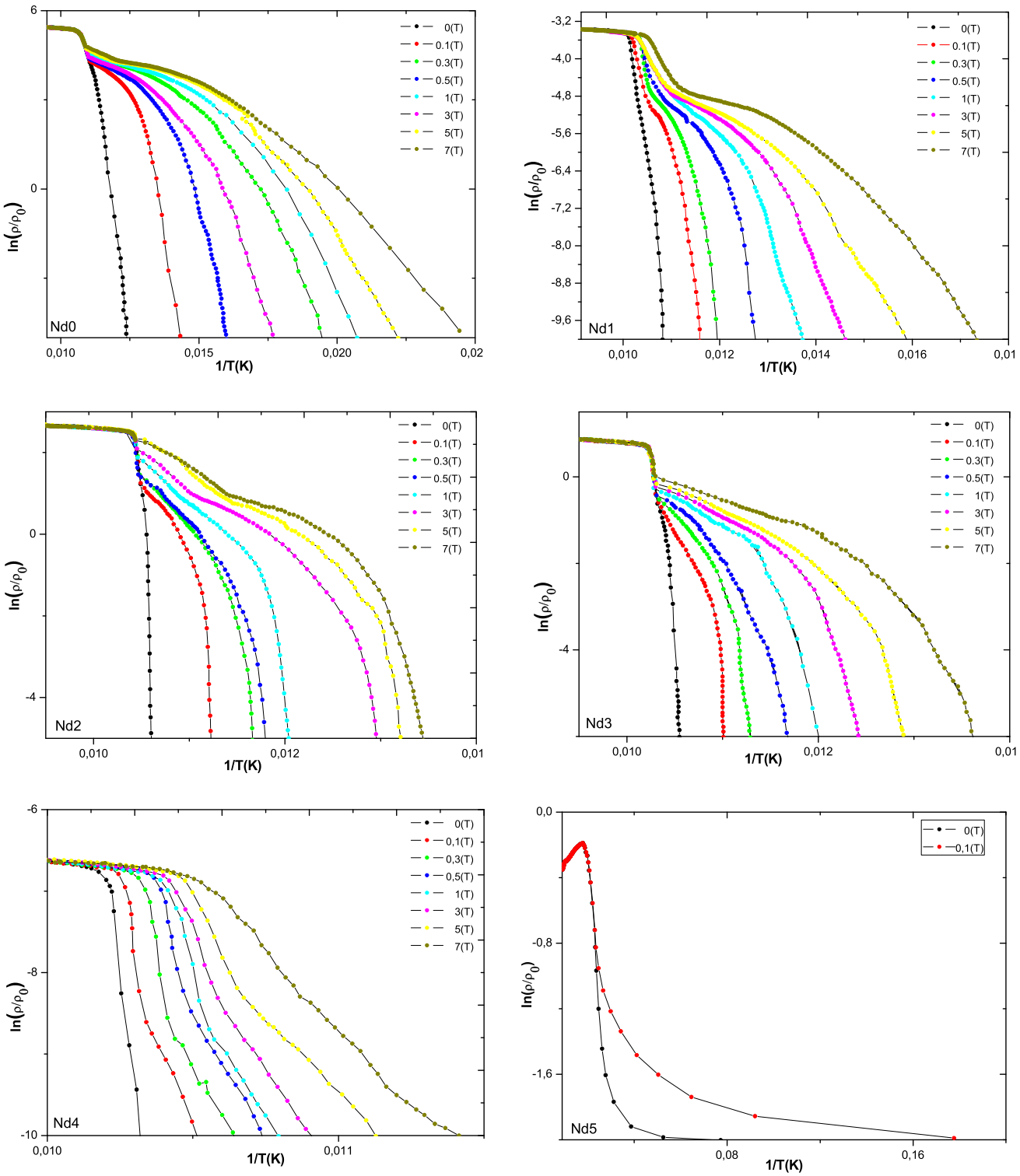

Fig. 2 $\ln(\rho/\rho_0)$ versus 1/T graphs of the bulk Y-123 superconducting materials

Table 2. The reduction of β value stems from the destruction of grain boundary weak interactions in the inter-granular coupling. It is noteworthy that the Nd0 (Nd4) compound exhibits least sensitivity (most sensitivity) to the applied magnetic field. Unfortunately, we cannot determine the β value belonging to the Nd5 compound due to the lack of the magnetic characteristics under the applied field which is larger 0.1 T. It is fair to conclude that the Nd

Table 2 Activation energy and β values of the pure and Ba-site Nd substituted Y-123 superconductors

Samples	Activation energies (K)								β values
	0 T	0.1 T	0.3 T	0.5 T	1 T	3 T	5 T	7 T	
YNd0	820	569	352	271	196	134	110	91	0.486
YNd1	1444	908	570	436	311	199	163	133	0.438
YNd2	2107	1342	907	719	477	333	279	210	0.401
YNd3	3028	1785	1250	1030	680	485	405	311	0.334
YNd4	6997	2553	1785	1417	1028	693	570	477	0.307
YNd5	86	53	Not measurable						

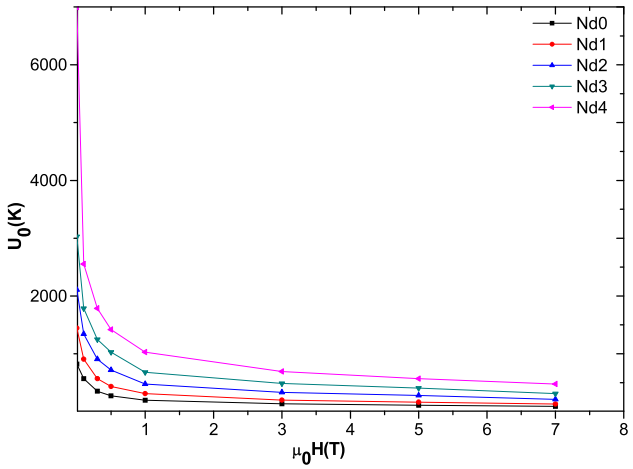

Fig. 3 Variation of flux pinning energy over different magnetic fields up to 7 T for the Nd samples

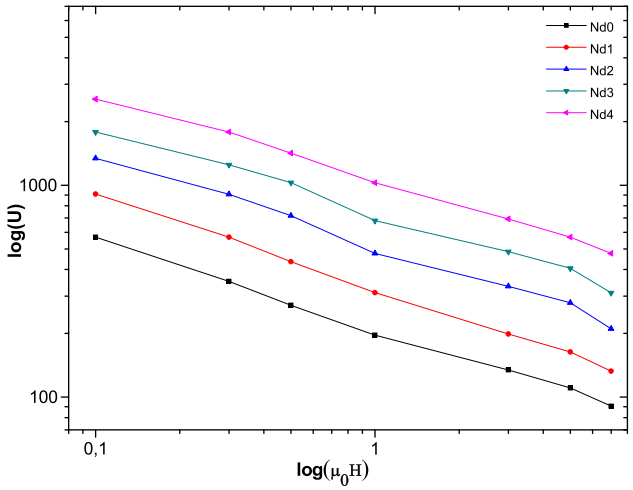

Fig. 4 External magnetic field dependence of flux pinning energy (U_0) for the inorganic solid compounds

nanoparticles are ploughed to improve the flux pinning ability, electrical and superconducting properties for the Y-123 matrix. To sum up, the excess Nd individuals give rise to deteriorate the correlation between copper oxide planes. In fact the excess impurities ($x > 0.250$) destroy the Y-123 superconducting lattice.

3.3 Irreversibility and upper critical field

The high temperature superconducting samples at the magnetic field applied confirm that each superconducting material attains negative surface energy playing an important role to form the quantized fluxoids on the specimen surface, and thus superconductivity in the structure does not abolish altogether, in contrast, retrogrades gradually at even higher applied magnetic field. This fact can be verified by the presence of the H_c, H_{c1}, H_{c2} and H_{c3} parameters. Magnetic field up to the value of H_{c1} is completely expulsed by the material exhibiting Meissner behavior [61] and the irreversibility fields related to H_{c1} are obtained by means of the following relation [62]:

$$H_{irr} \cong 200 \times H_{c1} \tag{2}$$

Moreover, the field strength between H_{c1} and H_{c2} values penetrates partially in the form of quantized vortices within fluxoids and the materials enter in a special state referred as mixed state or Schubnikov phase [63]. At the applied critical field of H_{c2}, the average field in the interior equals to the external magnetic field applied and the second-order phase transition occurs in the system; that is, the bulk superconductivity disappears completely. At fairly greater field applied ($H_{c3} > H > H_{c2}$), the superconductivity in a thin surface layer appears only. In other words, the surface sheath of the superconducting compound persists to rather greater critical field that is named as $H_{c3} \approx 1.69\ H_{c2}$ [34]. Additionally, in type-II superconductors there is another crucial field known as the thermodynamic critical field (H_c) that is in association with the measure of the extent to which the superconducting state is favored over normal state in the lack of magnetic field and can be extracted from the formula given below:

$$H_{c1} = \frac{H_c^2}{H_{c2}} \tag{3}$$

All the critical field parameters given above can be determined by several experimental methods including the

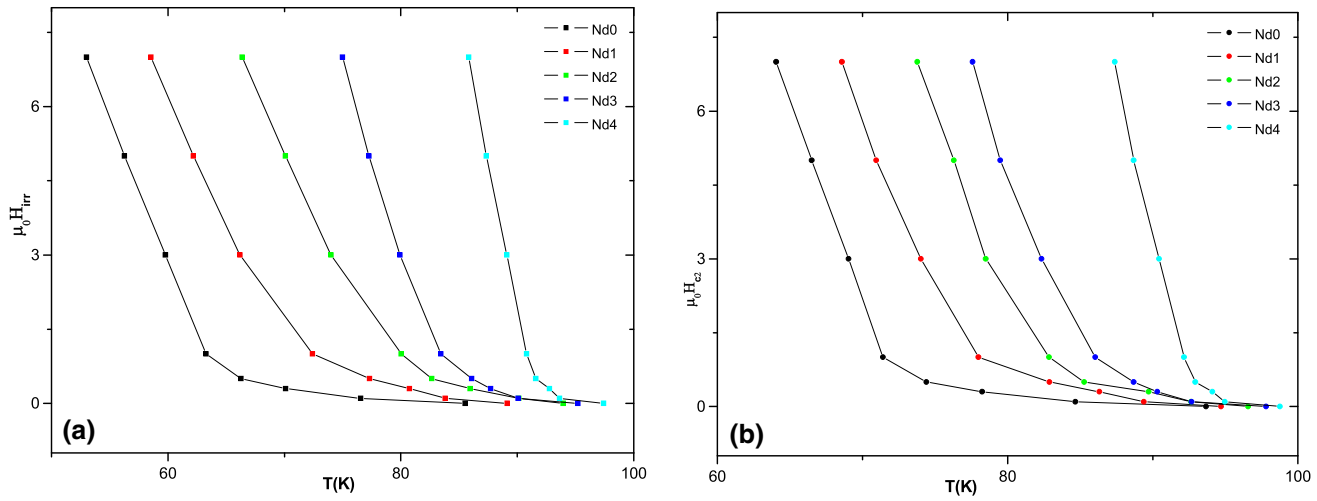

Fig. 5 Temperature dependences of **a** Irreversibility fields ($\mu_0 H_{irr}$) and **b** Upper critical fields ($\mu_0 H_{c2}$)

resistive transition $\rho(\mu_0 H, T)$, ac susceptibility and dc magnetization techniques to obtain the information about the vortex dynamics of the systems [64, 65]. In the present work, the resistive transition $\rho(\mu_0 H, T)$ measurements give an advantage that the systematic survey of the applied magnetic field on the resistive transitions simplifies to discuss the change in the vortex dynamics of new superconducting system [66, 67].

Temperature-dependent resistivity at the constant of the external field is obtainable as the following relations [68, 69],

$$\rho(\mu_0 H_{irr}, T) = 0.1\rho_n \text{ for the } \mu_0 H_{irr}(T) \quad (4)$$

and

$$\rho(\mu_0 H_{c2}, T) = 0.9\rho_n \text{ for the } \mu_0 H_{c2}(T) \quad (5)$$

where ρ_n is related to the normal state resistivity values concerning to the inorganic solid compounds at the temperature value of 95 K. The intercepts of extrapolation to zero point on the temperature axis for the values of $\mu_0 H_{irr}$ (T) and $\mu_0 H_{c2}$ (T) ascribe to the direct values of $\mu_0 H_{irr}$ (0) and $\mu_0 H_{c2}$ (0), respectively [70].

It is obvious from the Fig. 5 that the $\mu_0 H_{irr}$ and $\mu_0 H_{c2}$ curves shift to far lower temperature values with the increment in the Nd impurity content level after $y = 0.250$ as a result of the reduction in the flux pinning force [71]. In the case of the content level of $y = 0.500$, we cannot evaluate the full set values of the $\mu_0 H_{irr}$ and $\mu_0 H_{c2}$ parameters. This is in accordance with the fact that the excess Nd content level in the Y-123 superconducting matrix demolishes the pinning ability completely due to the shrink of distance between the pinning centers.

At the same time, the theoretical results found are numerically listed in Table 3 in detail. It is visible from the table that the $\boldsymbol{H_{irr}}$ parameters vary from 764.50 T (for the pure sample) to 76.39 T (for the Nd4 material). This result is another clue of the degradation of the flux pinning ability with the increase of the Nd concentration level in the Y-123 superconducting system owing to the existence of the Cooper pair-breaking mechanism.

As for the H_{c3} and H_c values calculated for the materials, there seems to be similar trend in the change of the H_{c3} and H_c parameters in the presence of the Nd nanoparticles in the Y-123 crystal structure. The smallest values ascribe to the sample prepared by the maximum Nd concentration inserted in the Y-123 lattice. In other words, the excess Nd impurity makes rapidly the phase translation from the superconducting state to normal state of the Y-123 structure, confirming strongly both the decrease of Josephson coupling length and increase in the elastic moduli of the vortex lattice.

3.4 Coherence length, penetration depth and Ginzburg–Landau parameter

One of the important properties of coherence length is impurity of samples. If there is impurity, coherence length increases. Secondary phase in samples are effective for critical current. These phases behave like flux trap center and increase coherence length. When the coherence length is greater than 2 nm, critical current density increases.

Coherence length of superconductor in perfect impurity is abbreviated ξ_0 and is also intrinsic characteristic properties of superconductor. ξ_0 value is formulated by Pippard as following;

$$\xi_0 \approx (\hbar v_f / \pi \Delta(0)) \approx 0.18(\hbar v_f / k_B T_c) \quad (6)$$

where k_B is Boltzmann constant, $\Delta(0)$ is change in energy of sample that is superconductor at absolute 0 K and v_f is velocity of electrons at Fermi energy level.

Table 3 Temperature-independent critical field parameters (μ_0H_{c1}, μ_0H_c, μ_0H_{irr}, μ_0H_{c2} and μ_0H_{c3}) and extracted λ, ξ and κ values belonging to the superconducting samples at absolute zero temperature

Samples	$H_{c1}(0)$ (T)	$H_{irr}(0)$ (T)	$H_{c2}(0)$ (T)	$H_{c3}(0)$ (T)	$\xi(0)$ (Å)	$\lambda(0)$ (Å)	$\kappa(0)$
YNd0	3.82	764.50	824.05	1392.64	6.32	6.56	1.04
YNd1	1.13	225.01	235.2	397.49	11.84	12.10	1.02
YNd2	0.52	104.60	191.72	324.01	13.11	17.75	1.35
YNd3	0.38	76.95	134.48	227.27	15.66	20.70	1.32
YNd4	0.38	76.39	121.58	205.47	16.47	20.77	1.26

On the other hand, the coherence length is attributed to a cylindrical core of a radius ξ whereas the penetration depth is in related to a current circulating around the core out to a distance λ [72]. Hence, theoretical calculations including the upper critical magnetic field and irreversibility fields allow us to find the $\xi(0)$ and $\lambda(0)$ values at the absolute zero temperature as the following relations:

$$\xi(T) = \left[\frac{\phi_0}{2\pi\mu_0 H_{c2}(T)}\right]^{\frac{1}{2}} \text{ and } \lambda(T) = \left[\frac{\phi_0}{2\pi\mu_0 H_{irr}(T)}\right]^{\frac{1}{2}} \quad (7)$$

where the vale of ϕ_0 is equal $2.07 \times 10^{-15} Tm^2$. The parameter values of $\xi(0)$ and $\lambda(0)$ are shown in Table 3. It is said from the given table that both the $\xi(0)$ and $\lambda(0)$ parameters have a tendency to continuously fall with the enrichment of the Nd content level up to $y = 0.250$ in the Y-123 superconducting lattice and actually reach the lowest value $\xi(0)$ of 16.47 Å and $\lambda(0)$ of 20.77 Å for the Nd4 sample. This is correlated to the fact that the Nd inclusion in the superconducting structure is favorable for the velocity of the Y-123 phase formation and it is reasonable to conclude that the superconducting quantities pertaining to the Y-123 ceramics develop with the rise of the Nd nanoparticles. It is another possible result that the considerable increment in the penetration depth (relative to the coherence length) is the result of the reduced mean free path with the excess Nd concentration level (after $y = 0.250$). The change of the ratio between the coherence length and penetration depth is defined as Ginzburg–Landau parameter abbreviated as κ at only vicinity of the absolute zero temperature. It is pertinent to mention here that for the type II superconducting materials the value of κ is almost constant along the whole temperature range study. According to the results, all the compounds produced exhibit London type superconductors in electrodynamics locality as a result of the higher κ value of $\frac{1}{\sqrt{2}}$ and also the regular enhancement in the κ value with the excess Nd content level suppresses the superconductivity as shown in the Nd5 specimen.

4 Conclusion

Although some similarities between $YBa_{2-y}Nd_yCu_3O_7$ and YBCO structures do exist, there are also incredible differences in their magnetic behaviour. Below the T_c, the magnetic flux can generally enter hard the $YBa_{2-y}Nd_yCu_3O_7$ compounds into its vortex region ($H_{c1} < H < H_{c2}$) and greater amount of fields can be trapped than in pure YBCO.

When we viewed the variable magnetic field and temperature graphs, decline of T_c^{offset} became more pronounced by increasing the applied magnetic field. This situation arises due to be non-superconducting phase in the superconducting particles of samples and weak links caused by the presence of porosity between the particles. Magnetic field begins to enter into the weak links boundary of samples and causes the negative effect on superconductivity. Also, if Nd impurity is considered to have great magnetic moments and to be a strong magnetic ion, magnetization or interior field is increased by these magnetic moments that try to get themselves through the direction of increasing field applied. As a result, the superconductivity will be affected negatively. This is known as the main reason for the decline in T_c^{offset}.

In this comprehensive study, we struggle to examine the variation of the flux pinning ability, electrical and superconducting characteristics of the Y-123 superconducting compounds with respect to the Nd concentration level ($0 \leq x \leq 0.500$) in the crystal structure via the magneto-transport measurements exerted in the external field range from 0 to 7 T. The main aim of the study is to obtain the regular consecutively stacked layers in order to develop both the pinning of 2D pancake vortices and the interlayer Josephson coupling by the partial replacement of Ba by Nd impurities in the system. Hereafter, the thermal fluctuation and interplane interaction energy of pancake vortices reduce noticeably and the end, the magnetic field carrying capacity is meaningfully improved by the increment of Josephson coupling length. According to the magnetoresistivity measurement, the room temperature resistivities, residual resistivity ratios, critical transition temperatures, penetration depths and coherence lengths, irreversibility fields, upper critical fields, thermodynamic critical fields, activation energies approve the regular enhancement in the flux pinning abilities of the Y-123 superconducting materials with the addition in the Nd concentration level up to $y = 0.250$ as a result of the regular distribution of the artificial pinning centers. Furthermore, the noteworthy conclusions from the current work are as the followings:

- The residual resistivity values tend to decrease systematically with arising the Nd nanoparticles up to y = 0.250 as a consequence of the decrement in the superconducting grain boundaries, voids, stacking faults, planar and micro defects in the Cu–O_2 planes. After y = 0.250, the specimen quality diminishes regularly owing to the lessening of the conductivity between the superconducting layers, that is localization problems in the conduction band, being even confirmed by the change in the normal state resistivity values belonging to the bulk Y-123 materials.
- Likewise, both the T_c^{onset} and T_c^{offset} values fall fast with the excess Nd inclusions due to both the distortion between Y-123 superconducting layers, and the formation of the porosities and weak-links between the superconducting grains. Reduction of the structural inhomogeneities in the oxidation state of the grains and grain boundaries is another feasible evidence for the decrement in T_c^{onset} and T_c^{offset} parameters with the Nd decorations. Similarly, the applied magnetic field damages melodramatically the critical transition temperatures and in fact we cannot measure the temperature values for the Nd5 (exposed to excess Nd impurities) sample at higher external magnetic field value such as 0.1 T. This is in association with the Cooper pair-breaking mechanism described as the hybridization of Nd5 states with the Cu3d–O_2p states in the Cu–O_2 layer, being favored by the degree of the broadening. Numerically, the T_c^{onset} values decrease from 94.69 K towards 54.84 K whereas the T_c^{offset} values change in the range of 84.52–32.97 K with increasing the Nd concentration level at zero applied magnetic field. However, the T_c^{offset} value of the best (Nd4) sample reduces to 82.04 K at the applied filed of 7 T while we cannot measure the values for the Nd5 material at higher applied magnetic field then 0.1 T.
- The activation energy changes are similar in the change of the critical temperatures. To be precise, the flux pinning energy values comprehended from the TAFF model tend to decrease from 6997 to 477 K with external magnetic field applied for the best sample (Nd5) due to the increment in the thermal fluctuations. This is correlated to the extensive regression of the pinning of 2D pancake vortices with the randomly distributed Nd inclusions in the Y-123 superconducting lattice. In other words, the recoupling linelike feature among the Cu–O_2 slabs improves quickly and the adjacent layers desire decoupling hastily. Therefore, both the interlayer Josephson coupling length and elasticity of the vortex lattices suppress in the system.
- Additionally, variation of the activation energies against the applied magnetic field shows that the sensitivity of the materials to the external field increases recurrently as a result of the demolition of the weak interactions in the inter-granular couplings.
- As for the other theoretical findings obtained, the critical field parameters as regards μ_0H_c, μ_0H_{c1}, μ_0H_{irr}, μ_0H_{c2} and μ_0H_{c3} and the extracted λ, ξ and κ values each present the degradation of the flux pinning ability with the Nd concentration owing to the presence of the random distribution of the artificial pinning centers and Cooper pair-breaking mechanism.

All in all, it is not wrong to assert that the Nd inclusions up to x = 0.250 are ploughed to improve the flux pinning ability, electrical and superconducting characteristics of the Y-123 superconducting texture.

Acknowledgments This study is partially supported by Abant Izzet Baysal University Scientific Research Project Coordination Unit (Project No: 2013.09.03.655).

References

1. P.M. Sarun, S. Vinu, R. Shabna, A. Biju, U. Syamaprasad, Mater. Res. Bull. **44**, 1017–1021 (2009)
2. N.K. Sarıtekin, Y. Zalaoglu, G. Yildirim, M. Dogruer, C. Terzioglu, A. Varilci, O. Gorur, J. Alloys Compd. **610**, 361–371 (2014)
3. H. Miao, M. Meinesz, B. Czabai, J. Parrell, S. Hong, AIP Conf. Proc. **986**, 423–430 (2008)
4. M. Runde, IEEE Trans. Appl. Supercond. **5**, 813–816 (1995)
5. A.V. Narlikar, C.V.R. Narasimha, S.K. Agarwal, in *Studies of High Temperature Superconductors, Advances in research and applications*, ed. by A. Narlikar (Nova Science Publishers, New York, 1989), p. 1
6. N.K. Sarıtekin, M. Dogruer, G. Yıldırım, C. Terzioglu, J. Mater. Sci. Mater. Electron. **25**, 3127–3136 (2014). doi:10.1007/s10854-014-1993-0
7. P. Karen, H. Fjellvag, A. Kjekshus, A.F. Andresen, Solid State Chem. **92**, 57–67 (1991)
8. R.J. Cava, J. Am. Ceram. Soc. **83**(1), 5–28 (2000)
9. Y. Zalaoglu, G. Yildirim, H. Buyukuslu, N.K. Saritekin, A. Varilci, C. Terzioglu, O. Gorur, J. Alloys Compd. **631**, 111–119 (2015)
10. N.K. Saritekin, M. Pakdil, G. Yildirim, M. Oz, T. Turgay, J. Mater. Sci. Mater. Electron. (2015). doi:10.1007/s10854-015-3839-9
11. N.K. Saritekin, C. Terzioglu, M. Pakdil, T. Turgay, G. Yildirim, J. Mater. Sci. Mater. Electron. (2015). doi:10.1007/s10854-015-3964-5
12. M. Oussena, P.A.J. de Groot, R. Gagnon, I. Taillefer, Phys. Rev. Lett. **72**, 3606 (1994)
13. A. Erb, E. Walker, J.Y. Genoud, R. Flükiger, Phys. C **282–287**, 2145–2146 (1997)
14. A. Erb, A.A. Manuel, M. Dhalle et al., Solid State Commun. **112**, 245 (1999)
15. M. Daeumling, J.M. Seuntjens, D.C. Larblestier, Nature **346**, 332 (1990)
16. H.W. Weber, in *Handbook on the Physics and Chemistry of Rare Earths*, ed. by K.A. Gscheidner Jr, I. Eyring, M.B. Maple (Elsevier, Amsterdan, 1999)

17. S. Vinu, P.M. Sarun, R. Shabna, U. Syamaprasad, J. Alloys Compd. **487**, 1–4 (2009)
18. M.H. Pu, W.H. Song, B. Zhao, X.C. Wu, Y.P. Sun, J.J. Du, J. Fang, Phys. C **361**, 181–188 (2001)
19. M. Dogruer, Y. Zalaoglu, A. Varilci, C. Terzioglu, G. Yildirim, O. Ozturk, J. Supercond. Nov. Magn. **25**, 961–968 (2012)
20. N.K. Sarıtekin, M. Dogruer, Y. Zalaoglu, G. Yıldırım, C. Terzioglu, O. Gorur, J. Alloys Compd. **659**, 31–37 (2016)
21. G.L. Bhalla, A. Malik Pratima, K.K. Singh, Phys. C **391**, 17–24 (2003)
22. Y. Eltsev, S. Lee, K. Nakao, S. Tajima, Supercond. Sci. Technol. **23**, 55007 (2010)
23. N.T. Mua, A. Sundaresan, N.K. Man, D.D. Dung, Bull. Mater. Sci. **37**, 19–25 (2014)
24. M. Li, Y. Zhang, Y. Li, Y. Qi, J. Non-Cryst. Solids **356**, 2831–2835 (2010)
25. G. Yildirim, S. Bal, E. Yucel, M. Dogruer, M. Akdogan, A. Varilci, C. Terzioglu, J. Supercond. Nov. Magn. **25**, 381–390 (2012)
26. O. Ozturk, E. Asikuzun, M. Erdem, G. Yildirim, O. Yildiz, C. Terzioglu, J. Mater. Sci. Mater. Electron. **23**, 511–519 (2012)
27. A.A. Abrikosov, L.P. Gor'kov, Zh. Eksp. Teor. Fiz. **39**, 1781–1796 (1960)
28. Y. Dalichaouch, M.S. Torikachvilli, E.A. Early, B.W. Lee, C.L. Seaman, K. Yang, H. Zhou, M.B. Maple, Solid State Commun. **65**, 1001–1006 (1988)
29. B. Okai, M. Kosuge, H. Nozaki, K. Takahashi, M. Ohta, Jpn. J. Appl. Phys. **27**, L41–L44 (1988)
30. D.P. Norton, D.H. Lowndes, J.D. Budai, B.C. Chakoumakos, H.R. Kerchner, Phys. Rev. Lett. **66**, 1537–1540 (1991)
31. X.X. Tang, A. Manthiram, J.B. Goodenough, Phys. C **161**, 574–580 (1989)
32. P. Wei, H.W. Ying, Z.Q. Qi, Phys. C **209**, 400–406 (1993)
33. J.J. Neumeier, T. Bjormholm, M.B. Maple, I.K. Shuller, Phys. Rev. Lett. **63**, 2516–2519 (1989)
34. J.J. Neumeier, M.B. Maple, Phys. C **191**, 158–166 (1992)
35. A. Mourachkine, *Room-Temperature Superconductivity*, 2nd edn. (Cambridge International Science Publishing, Cambridge, 2004)
36. A.E. Koshelev, P. LeDoussal, V.M. Vinokur, Phys. Rev. B Condens. Matter **53**, R8855–R8858 (1996)
37. G. Yildirim, M. Dogruer, F. Karaboga, C. Terzioglu, J. Alloys Compd. **584**, 344–351 (2014)
38. D.M. Newns, P.C. Pattnaik, C.C. Tsuei, Phys. Rev. B Condens. Matter **43**, 3075–3084 (1991)
39. M.B. Turkoz, S. Nezir, C. Terzioglu, A. Varilci, G. Yildirim, J. Mater. Sci. Mater. Electron. **24**, 896–905 (2013)
40. R. Kalyanaraman, S. Oktyabrsky, J. Narayan, J. Appl. Phys. **85**, 6636–6641 (1999)
41. F. Rullier-Albenque, P.A. Vieillefond, H. Alloul, A.W. Tyler, P. Lejay, J.F. Marucco, Europhys. Lett. **50**, 81–87 (2000)
42. X. Xu, J.H. Kim, S.X. Dou, S. Choi, J.H. Lee, H.W. Park, M. Rindfleish, M. Tomsic, J. Appl. Phys. **105**, 103913 (2009)
43. C. Autret-Lambert, B. Pignon, M. Gervais, I. Monot-Laffez, A. Ruyter, L. Ammor, F. Gervais, J.M. Bassat, R. Decourt, J. Solid State Chem. **179**, 1698–1706 (2006)
44. C.B. Dennis, *Elements of X-Ray Diffraction*, 3rd edn. (N.J. Prentice Hall, London, Prentice-Hall International, Upper Saddle river, 2001)
45. A.D. Bustamante, A.A. Osorio, L.V. De Los Santos et al., Adv. Sci. Technol. **47**, 37–42 (2006)
46. M.R. Koblischka, A.J.J. van Dalen, T. Higuchi, K. Sawada, S.I. Yoo, M. Murakami, Phys. Rev. B **54**, R6893 (1996)
47. G. Krabbes, G. Fuchs, P. Schätzle et al., Phys. C **330**, 181 (2000)
48. G. Fuchs, A. Gladun, K. Fischer, C. Rodig, Cryogenics **32**, 591 (1992)
49. R.I. Peterson, J.W. Ekin, Phys. Rev. B **42**, 8014 (1990)
50. Y. Yeshurun, A.P. Malozemoff, Phys. Rev. Lett. **60**, 2202 (1988)
51. M.V. Feigelman, V.B. Geshkenbein, A.I. Larkin, V.M. Vinokur, Phys. Rev. Lett. **63**, 2303–2306 (1989)
52. M.P.A. Fisher, Phys. Rev. Lett. **62**, 1415–1418 (1989)
53. V.V. Schmidt, P. Muller, A.V. Ustinov, I.V. Grigorieva, *The Physics of Superconductors: Introduction to Fundamentals and Applications*, 1st edn. (Springer, Berlin, 2010)
54. G. Yildirim, M. Akdogan, S.P. Altintas, M. Erdem, C. Terzioglu, A. Varilci, Phys. B **406**, 1853–1857 (2011)
55. I. Kusevic, E. Babic, Z. Marohnic, J. Ivkov, S.X. Dou, Phys. C **235–240**, 3035–3036 (1994)
56. M. Dogruer, O. Gorur, Y. Zalaoglu, O. Ozturk, G. Yildirim, A. Varilci, C. Terzioglu, J. Mater. Sci. Mater. Electron. **24**, 352–361 (2013)
57. E. Govea-Alcaide, I. Garcia-Fornaris, P. Mune, R.F. Jardim, Eur. Phys. J. B **58**, 373–378 (2007)
58. P. Muné, E. Govea-Alcaide, R.F. Jardim, Phys. C **384**, 491–500 (2003)
59. M.D. Sumption, M. Bhatia, S.X. Dou, M. Rindfliesch, M. Tomsic, L. Arda, M. Ozdemir, Y. Hascicek, E.W. Collings, Supercond. Sci. Technol. **17**, 1180–1184 (2004)
60. Y. Zalaoglu, G. Yildirim, C. Terzioglu, J. Mater. Sci. Mater. Electron. **24**(239–24), 7 (2013)
61. W. Meissner, R. Ochsenfeld, Naturwissenschaften **21**, 787–788 (1933)
62. T.P. Sheahen, *Introduction to High temperature Superconductivity* (Kluwer Academic Publishers, New York, 2002)
63. Y.N. Ovchinnikov, Usp. Fiz. Nauk **137**, 473–478 (1982)
64. L.T. Sagdahl, S. Gjolmesli, T. Laegreid, K. Fossheim, W. Assmus, Phys. Rev. B Condens. Matter **42**, 6797–6800 (1990)
65. S. Celebi, S. Nezir, A. Gencer, E. Yanmaz, M. Altunbas, J. Alloys Compd. **255**, 5–10 (1997)
66. T.T.M. Palstra, B. Batlogg, R.B. Van Dover, L.F. Schneemeyer, J.V. Waszczak, Phys. Rev. B Condens. Matter **41**, 6621–6632 (1990)
67. M. Tinkham, Phys. Rev. Lett. **61**, 1658–1661 (1988)
68. J.H. Kim, S.X. Dou, D.Q. Shi, M. Rindfleisch, M. Tomsic, Supercond. Sci. Technol. **20**, 1026–1031 (2007)
69. H. Kitaguchi, A. Matsumoto, H. Hatakeyama, H. Kumakura, Supercond. Sci. Technol. **17**, S486–S489 (2004)
70. C.S. Yadav, P.L. Paulose, New J. Phys. **11**, 103046 (2009)
71. N. Ojha, G.D. Varma, H.K. Singh, V.P.S. Awana, J. Appl. Phys. **105**, 07E315 (2009)
72. S.B. Guner, O. Gorur, S. Celik, M. Dogruer, G. Yildirim, A. Varilci, C. Terzioglu, J. Alloys Compd. **540**, 260–266 (2012)